ACS OMEGA

Open Access

http://pubs.acs.org/journal/acsodf

Article

Application of Hydrothermal Synthesized Titanium Dioxide-Doped Multiwalled Carbon Nanotubes on Filtration Properties—Response Surface Methodology Study

Muhammad Arqam Khan, Shaine Mohammadali Lalji, Syed Imran Ali, Mei-Chun Li,* and Muneeb Burney

Cite This: *ACS Omega* 2024, 9, 34765−34776

Read Online

ACCESS | Metrics & More | Article Recommendations

ABSTRACT: The success of any drilling activity mainly depends on the characteristics of the drilling fluid. Therefore, a high-performance drilling fluid is substantial for any drilling operation. During overbalance drilling operations, the drilling mud invades the permeable formations and causes the loss of circulation, which is responsible for nonproductive time events. Hence, the filtration characteristics of the drilling mud are an imperative property. The purpose of this study is to evaluate the filtration characteristics of water-based mud systems in the presence of polyanionic cellulose (PAC) and multiwalled carbon nanotubes (MWCNTs)/TiO_2 nanoparticles. The nanoparticles were synthesized by using the hydrothermal technique. For the first time, a composite of MWCNTs and TiO_2 has been utilized as a fluid loss control additive in the petroleum sector, marking a significant development in the field. The filtration properties of water-based mud were assessed at two concentrations (0.35 g and 3.5 g). Furthermore, based on the two levels (concentrations) and two factors (particles), the novel application of the central composite response surface design of experiment (CCD) was implemented. The results showed that the predicted model from CCD was in good agreement with the filter press experimental result with R^2 = 0.8446. Furthermore, based on the ANOVA analysis, the concentration of MWCNTs/TiO_2 nanoparticles was the most significant parameter with p-value < 0.05. In addition, 10 out of 13 experimental points fall under the ±10% error window, thus indicating a higher accuracy of the regression model. The 2D interactive plots further show that the concentration of PAC is insignificant and has no considerable influence on fluid loss control, which was also validated by p-value > 0.05. The performance of MWCNTs/TiO_2 nanoparticles is superior to PAC because these nanodimension particles plug the pore-spacing and block the permeation channels on the filter paper. However, the PAC, because of its long molecular chain, entangles around the pore spaces and plugs the microsize pores, which eventually reduces the filtration loss volume up to some extent. By observing the synergistic interaction between MWCNTs/TiO_2 nanoparticles and PAC, this study develops valuable insights that assist in improving the performance of drilling fluid and minimizes the wellbore instability issues in the oil and gas sector.

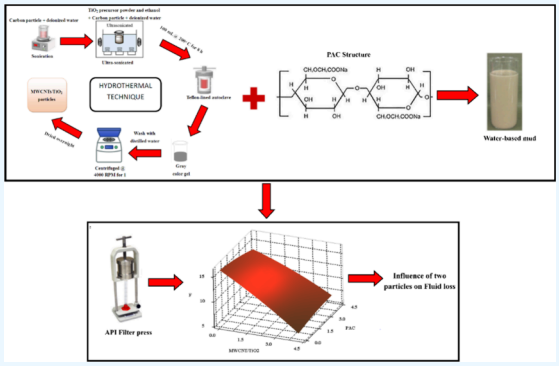

INTRODUCTION

The drilling activity is a fundamental process in the oil and gas sector.[1] This operation is predominantly dependent upon the performance of the drilling fluid, which plays an inimitable role during the drilling operations.[2] Drilling muds are mainly used to clean the wellbore by lifting the drilled cutting out of the borehole, keep the drill bit cool and lubricated, maintain the integrity of the borehole, and assist during wireline operations.[3,4] In general, drilling fluids are characterized into three main streams, namely; water-based mud (WBM), oil-based mud (OBM), and synthetic-based mud (SBM).[5] The SBM and OBM are more effective than WBM in terms of shale stability, rheological and filtration behavior, and high wellbore stability.[5,6] Nevertheless, factors like mud formulation, cost, and disposal are some major concerns that have severely impacted their use in the petroleum industry.[7] Therefore, WBM remains the most preferred option in drilling despite some deficiencies, especially in the form of shale swelling. This has instigated numerous researchers to concentrate on the upgrade of WBM performance and resolve fluid loss and shale disintegration problems.

Received: May 1, 2024
Revised: July 18, 2024
Accepted: July 24, 2024
Published: August 2, 2024

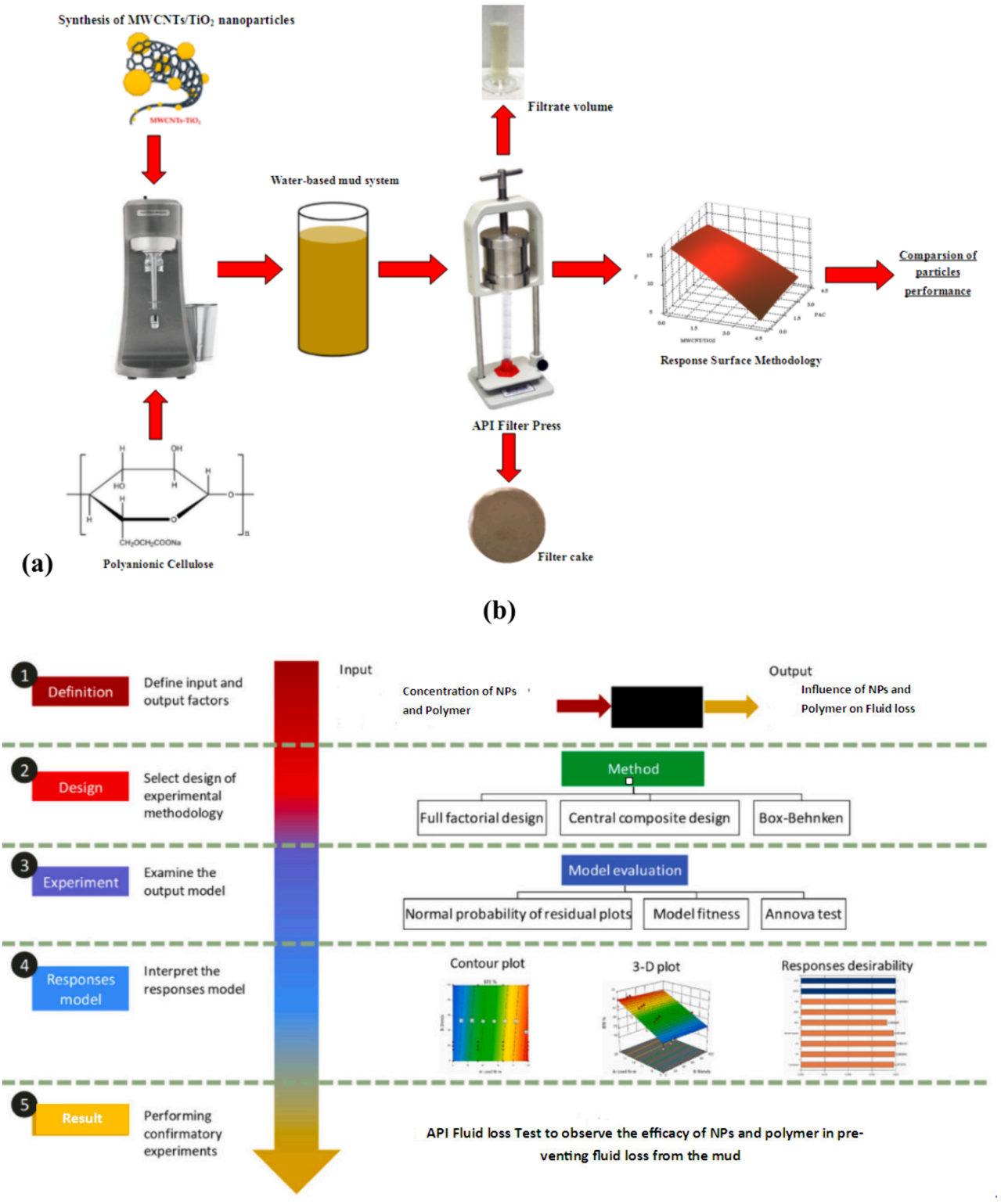

Figure 1. (a) Flowchart for the experimental procedure used in this study. (b) Flowchart of response surface methodology study. Reprinted from ref 30. Copyright 2023 Elsevier.

Several scholars have worked on the modification of WBM system properties by incorporating different additives, particularly salts.[3,8,9] However, studies have shown that at higher concentrations salt tends to dephase the mud system into two separate entities: sediments and liquids.[6,10] Therefore, the utilization of polymeric materials in the WBM system was broadened. These additives are used to minimize the shale disintegration, improve the rheological and filtration behavior, and obtain the desired viscosity that assists during drilling operations.[1,11,12] Overall, polymeric materials are classified as modified polymers, biopolymers, and synthetic polymers.[12]

Polyanionic cellulose (PAC) is a high-molecular-weight, modified polymer that consists of β-D-glucopyranose monomer units.[13] In drilling mud, PAC is commonly used as a fluid loss

https://doi.org/10.1021/acsomega.4c04177
ACS Omega 2024, 9, 34765−34776

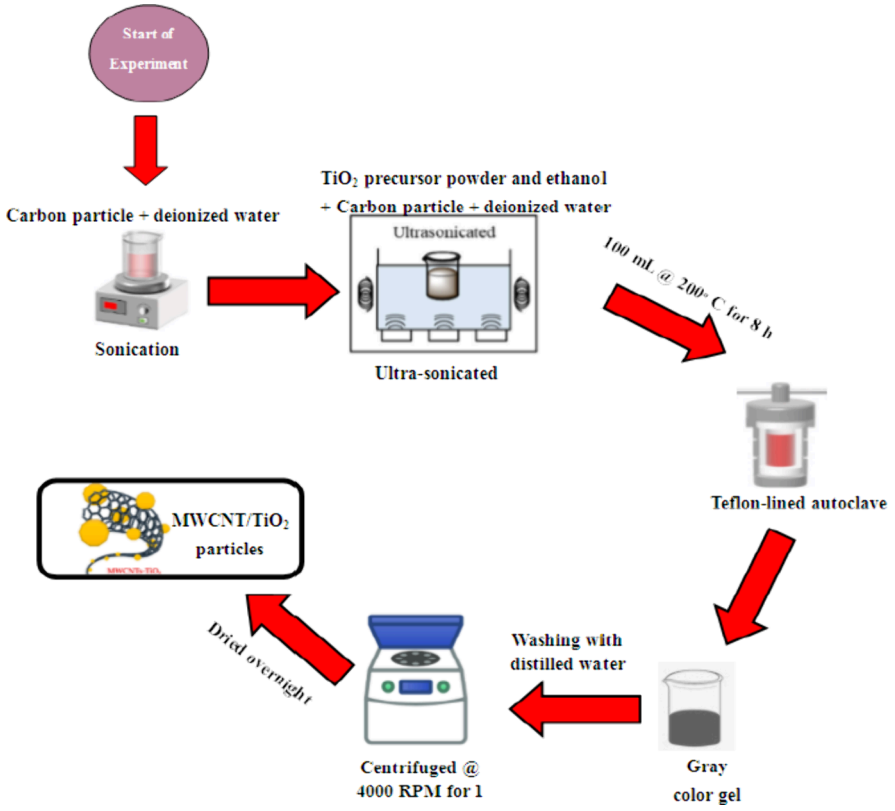

Figure 2. Schematic showing the synthesis of MWCNT/TiO_2 nanoparticles. Reprinted from ref 32. Copyright 2024 Springer.

control additive.[14] Moreover, it increases the thermal stability of the mud and can also work as an antibacterial agent.[14] Furthermore, PAC, when it became part of the WBM system, improves the filtration characteristics of the mud. Reduction in fluid loss was recorded by scholars working with this additive.[15] However, at high temperature and pressure conditions, PAC is not conducive. Additionally, this polymeric material suffers thermal degradation when used as a separate entity; hence, researchers combined it with various other additives to improve its characteristics.[14,16] On the basis of the shortcomings, the petroleum industry is investigating new techniques to establish efficient and effective drilling mud that can easily work in any drilling environment.[6] These new technologies have joined the petroleum sector in the form of nanoparticles.

The application of nanomaterials in the oil and gas sector has considerably improved the drilling performance. The nanoscale dimensions substantially increase the drilling productivity by enhancing the thermal, rheological, filtration, lubricity, and mechanical and chemical properties of the mud system.[6,17−19] In recent times, the application of different nanoparticles, such as graphene oxide,[20] zinc oxide,[17] iron oxide,[21] copper oxide,[22] and titanium dioxide (TiO_2),[23] and carbon nanotubes[24] have substantially improved the drilling performance.

A limited number of studies have been performed on TiO_2 application in drilling fluid.[25] The efficacy of TiO_2 is mainly a function of its crystal structure, surface area, band gap energy, and its crystallinity.[26] TiO_2's physicochemical properties, because of its shape and crystal system, have gained substantial interest in diverse fields.[26] To further improve the activity of TiO_2, various support systems are implemented by various carbonaceous materials, silica, and alumina.[27] The most effective support system is provided by carbonaceous materials, especially activated carbon and multiwalled carbon nanotubes (MWCNTs). Carbon nanotubes (CNTs) are predominantly carbon compounds with unique physical structures.[28] CNTs are classified as multiwalled carbon nanotubes (MWCNTs) and single-walled carbon nanotubes (SWCNTs).[28] The high aspect ratio, surface area, and nanoscale dimensions set CNTs apart from other additives and make them a potential choice as a fluid control additive.[29]

During this study, implementation of the design of the experiment is done to investigate the efficacy of polymers and nanoparticles in controlling the fluid loss from the WBMs. PAC and MWCNTs/TiO_2 nanoparticles became part of WBMs, and the dominance of these two entities in controlling the fluid loss was investigated using the central composite response surface design of experiment (CCD). Despite their widespread application in the photocatalysis industry, the MWCNTs/TiO_2 nanocomposites have remained an unexplored segment in the oil and gas sector until now. This study pioneers the use of the MWCNTs/TiO_2 nanoparticles as a fluid loss control additive, which marks a substantial departure from its traditional applications and paves the way for possible revolution in the field. During this analysis, the concentration of polymer and nanoparticles was the main factor used in this investigation. It is the first study of its own that investigated the performance of PAC and MWCNTs/TiO_2 nanoparticles in fluid loss control through statistical analysis.

CENTRAL COMPOSITE RESPONSE SURFACE DESIGN OF EXPERIMENT (CCD)

The central composite response surface design of an experiment is by far the most utilized design of experimental

https://doi.org/10.1021/acsomega.4c04177
ACS Omega 2024, 9, 34765−34776

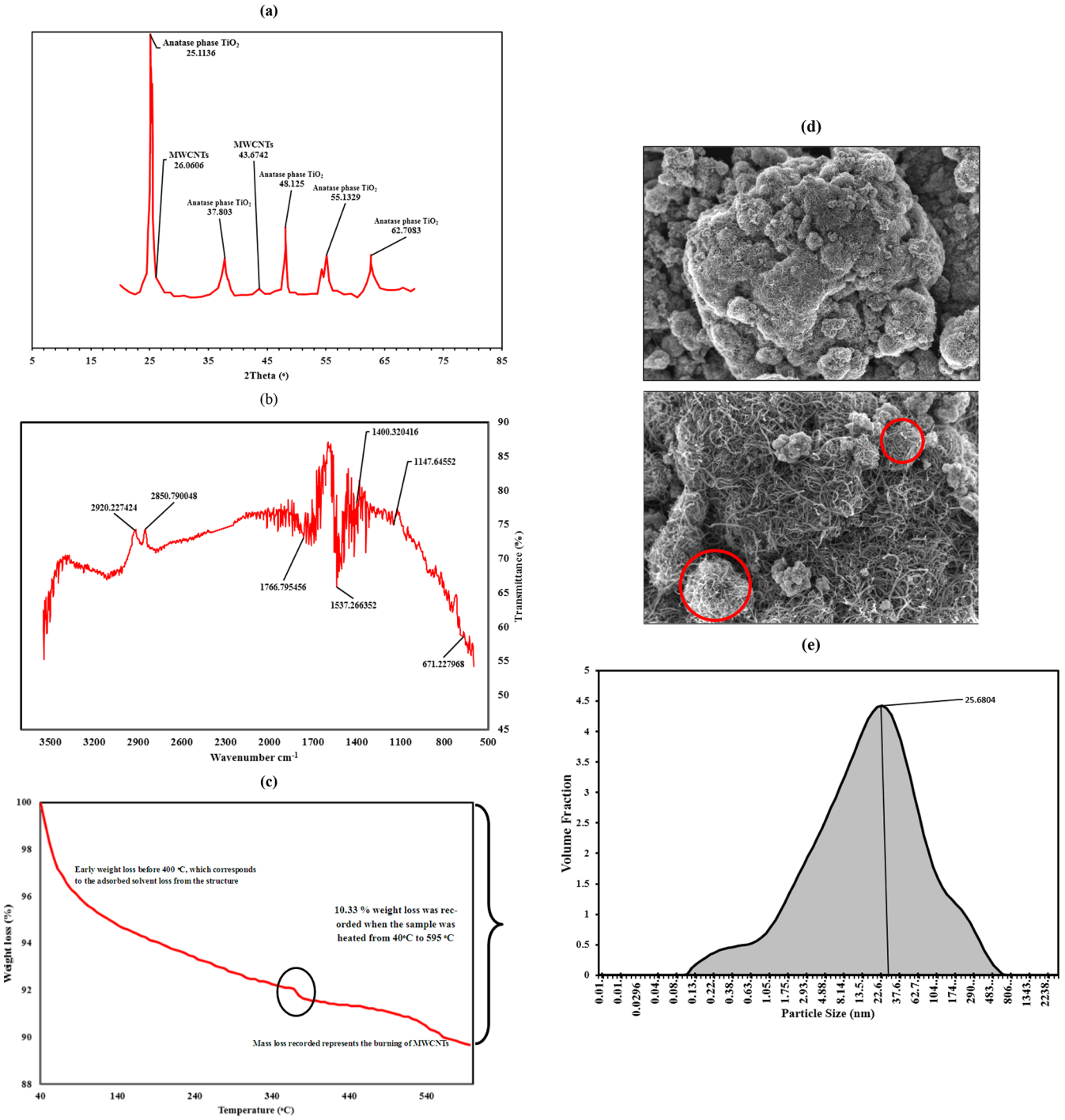

Figure 3. (a–e) Characterization of MWCNT/TiO_2 nanoparticles: (a) XRD spectrum, (b) FTIR, (c) TGA, (d) SEM imaging, and (e) particle size distribution.

methodology in different fields of applications. This design of experiment is extremely useful in sequential experimental analysis as it mainly focuses on the prior factorial investigations with the cooperation of center and axial points.[30] In addition, this methodology efficiently approximates first- and second-order terms and can effectively model a response feature with axial and center points. When compared with the Box–Behnken design (BBD), CCD provides excellent coverage for nonlinear relationships. Moreover, CCD contains an embedded factorial design that enables it to be more accurate for comprehensive model validation, flexible, and facilitate sensitivity analysis for chronological experimentation work than the Box–Behnken design.[30]

METHODOLOGY

Figure 1a shows the step-by-step flowchart followed in this study. The chart explains the complete study conducted in this article. Additionally, Figure 1b shows the response surface methodology (RSM) flowchart of the American Petroleum Institute (API) filter press test conducted in this article.

Synthesis of MWCNT/TiO_2 Nanoparticles. The carbonaceous-supported titanium dioxide (TiO_2) particles were

https://doi.org/10.1021/acsomega.4c04177
ACS Omega 2024, 9, 34765–34776

synthesized by using the hydrothermal method. The particles were successfully synthesized by following the protocols outlined by Muduli et al.[31] with some strategic modifications to optimize the process. Initially, a mixture of deionized water and carbonaceous material was agitated together in sonication for 90 min. Subsequently, a mixture containing titanium VI isopropoxide and ethanol was prepared, which was added dropwise into the carbonaceous material solution and agitated vigorously. The mixture was then placed into an ultrasonicated bath for 1 h. Afterward, the mixture removed from the ultrasonicated bath was placed into a 100 mL Teflon-lined autoclave and was heated at 200 °C for 8 h. During the synthesis of particles, it was ensured that the pH of the mixtures did not change drastically; hence, NaOH was added to the solution. After 8 h of heating, a gray-colored solution was obtained, which was washed several times with distilled water to remove any impure fractions. The product collected was then centrifuged at 4000 rpm for 1 h before drying overnight. The final product formed was carbon-supported titanium dioxide nanoparticles that were used as a drilling fluid additive to improve the performance of the WBMs. Figure 2 shows the experimental setup used in the preparation of the carbon-supported TiO_2 nanomaterials.

Characterization of MWCNT/TiO_2 Nanoparticles. The characterization of MWCNT/TiO_2 nanoparticles was done using XRD, FTIR, and TGA analysis, as shown in Figure 3a,c. The XRD spectrum is used to examine the crystalline quality of the carbon-supported anatase-TiO_2 particles. Figure 3a shows the XRD spectrum of carbon-supported anatase-TiO_2 particles. The diffraction spectrum obtained at 25.1136°, 37.803°, 48.125°, 55.1329°, and 62.7083° represents the existence of anatase crystal form of TiO_2 in all three carbon support particles. Moreover, the characteristic peaks at 26.30° and 43.6742° endorses the presence of MWCNTs. Figure 3b shows the Fourier transform infrared spectrum of the carbon-supported anatase-TiO_2 particles. This analysis represents the chemical bonding present within the molecules. The strong peaks at 2850.790 and 2920.227 cm^{-1} indicate the asymmetric and symmetric telescopic vibrations of the CH_2 group present in the carbon nanotubes. The peaks at 1147.645 and 1766.795 cm^{-1} represent the formation of carbonyl and carboxyl groups during the alteration process. The strong peak at 1537.266 cm^{-1} describes the stretching vibration of carbon double bonds present in the MWCNTs. Additionally, the peak at 671.227 cm^{-1} represents the absorption band of titanium dioxide. Figure 3c shows the thermal characteristics of the synthesized composite collected from thermogravimetric analysis (TGA). The sample was heated from 40 to 595 °C using the nitrogen flow, and the changes in the weight of the substance were recorded. The MWCNT/TiO_2 nanoparticles displayed an early weight loss before 400 °C, which corresponds to the adsorbed solvent loss from the structure. Another mass loss was also recorded between 350 and 595 °C. This loss represents the burning of MWCNTs. Overall, 10.33% weight loss was recorded when the sample was heated from 40 to 595 °C. Figure 3d shows the scanning electron microscope imaging of MWCNTs/TiO_2 nanoparticles obtained from a NOVA NanoSEM 450. With the help of the hydrothermal method, an interaction between TiO_2 nanoparticles and MWCNTs can be observed in SEM. According to the figure, higher concentrations of MWCNTs are embedded into the TiO_2 nanoparticles. The figure also shows a resilient interphase configuration effect between the MWCNT and TiO_2 nanoparticles. The MWCNTs formed a thin film over the TiO_2 nanoparticles, thus creating an explicit core−shell morphology. Figure 3e shows the particle size distribution of MWCNTs/TiO_2 nanoparticles. According to particle size distribution (PSD) analysis, the average particle size of the MWCNTs/TiO_2 nanoparticles was 25.68 nm. The particles were used as fluid loss control additives in the water-based drilling mud. Moreover, the influence of the particles on fluid loss characteristics was compared to polyanionic cellulose (PAC).

Preparation of Water-Based Mud System. The main aim of this study is to investigate the effect of MWCNT/TiO_2 nanoparticles and PAC in controlling the fluid loss volume from the WBM. A simple extended gel mud system was formulated in this study, which was modified through MWCNT/TiO_2 and PAC particles, respectively. The base mud consists of 324 mL of distilled water, 0.25 g of sodium carbonate, 15 g of viscosifiers in the form of bentonite, and 81 g of weighing agent barite. Table 1 shows the additives and their applications in the current study. All these additives were supplied by the Service Company currently operating in Pakistan. The additives used in the formulation of drilling mud were added sequentially to control fluid loss, viscosity, and mud cake formation. During the preparation of the water-based mud system, API standards were properly followed. Except for MWCNTs/TiO_2 nanoparticles, all of the remaining drilling fluid additives were delivered by a drilling service provider.

Table 1. Mud Additives with Their Molecular Weights and Functions in This Study

additive type	molecular weight (g/mol)	function	mixing time (minute)
distilled water	18	used as a continuous phase	
sodium carbonate	106	used for the treatment of water hardness	5
bentonite	180.1	viscosifiers	10
commercial polyanionic cellulose grade L	339 000	used as a filtrate loss control material	10
MWCNTs/TiO_2	56.1	used as a filtrate loss control material	10
barite ($BaSO_4$)	233	used to increase the density of mud	10

API Filter Press Test. The API filter press test was conducted according to the API protocols of 13B-1. The test was conducted at 30 °C and 100 psi. The mud sample was placed in an API cell, and a differential pressure of 100 psi was applied to the mud with the help of nitrogen gas. The test was conducted for 30 min. Whatman filter paper with a thickness of 115 μm was used to collect the mud cake and allow the filtrate loss to take place. During testing, it was ensured that the uncertainty in the testing procedure should remain below the desired limit of 2%.[33] In the API filter press experimentation, the uncertainty is mainly due to the differential pressure supplied across the cell, the reading of the graduated cylinder where filtrate is collected, and the thickness of the mud cake. Figure 4 shows the photographic representation of all of the mud cakes collected from the API filter press experiment. Each filter paper was laid under atmospheric conditions and was dried for 24 h. During this process, the evaporation of water molecules causes the filter paper to curl, which was tackled by

https://doi.org/10.1021/acsomega.4c04177
ACS Omega 2024, 9, 34765−34776

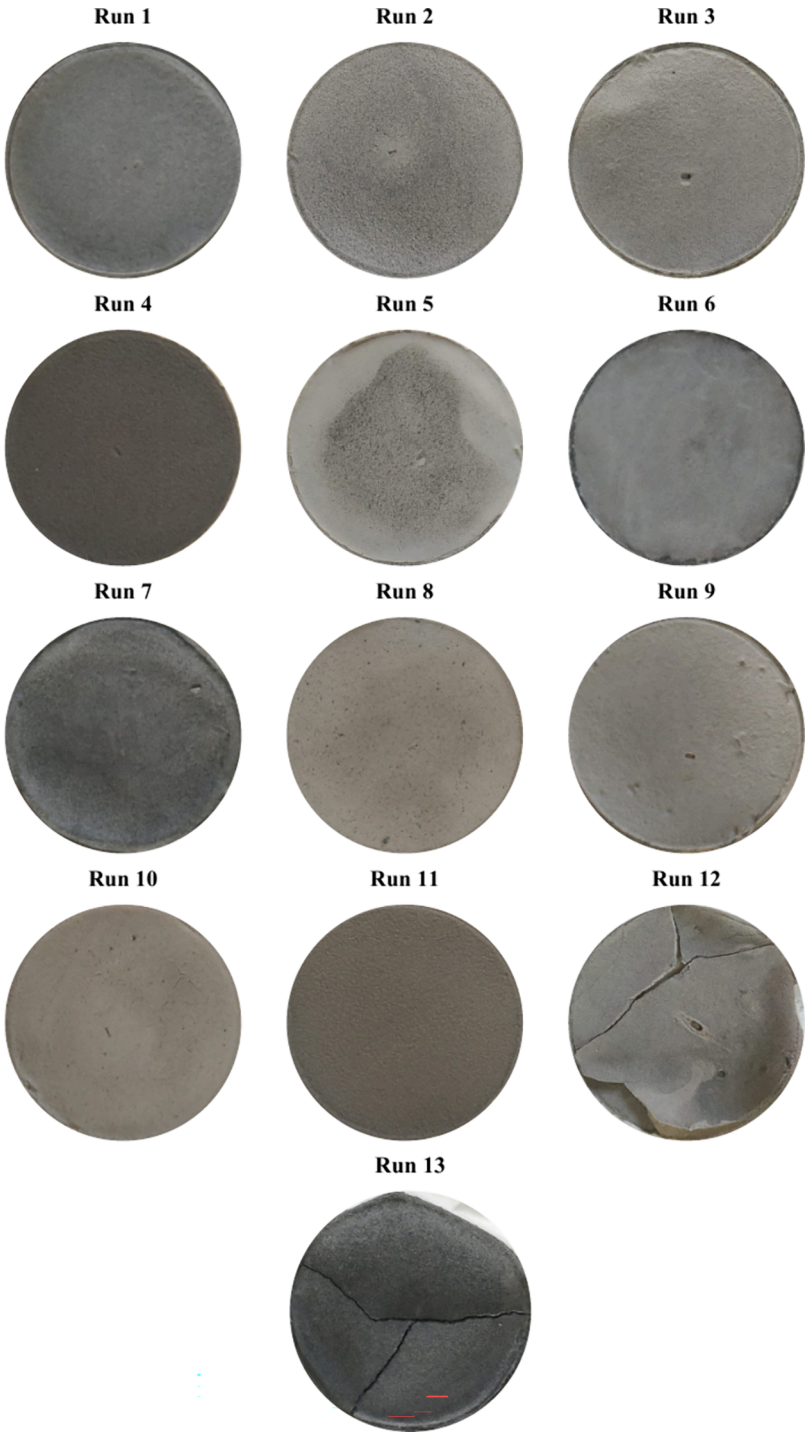

Figure 4. Filter cake of all 13 experiments from API filter press testing.

placing different weights on the filter paper. In the observation, the mud cake color becomes darker as the concentration of MWCNT/TiO_2 nanoparticles increases. Moreover, with MWCNT/TiO_2 nanoparticles, the mud cake was thin, dense, and compact with little or no cracks over its surface. The addition of MWCNT/TiO_2 nanoparticles seemed to improve the microstructure of the mud cake, which led to a more stable and impermeable mud cake. This eventually prevented fluid invasion and mitigated the wellbore instability issues. However, a higher concentration of PAC demonstrated a thick and lighter colored mud cake.

Design of Experiment (Response Surface Methodology). In this study, the central composite response surface design of the experiment method was followed. The influence of these particles on the filtrate loss was investigated, and the performance of particles was observed. The central composition design for the two factors MWCNT/TiO_2 and PAC is shown in Table 2. The design consists of two factors (MWCNT/TiO_2 and PAC) with two levels (0.35 and 3.5 g) of particles in the mud systems. In total, 13 runs were provided by the statistical software, and the actual values are shown in Table 2. The design is based on full factorial, which consists of

https://doi.org/10.1021/acsomega.4c04177
ACS Omega 2024, 9, 34765−34776

Table 2. Design of Experiment Matrix for Response Surface Methodology (RSM)

run	MWCNT/TiO_2 (g)	PAC (g)	F (mL)	run type
1	0.35	0.35	17.0	factorial points
2	3.50	0.35	10.0	
3	0.35	3.50	13.0	
4	3.50	3.50	8.0	
5	0.00	1.93	15.0	axial points
6	4.15	1.93	5.8	
7	1.93	0.00	9.0	
8	1.93	4.15	12.0	
9	1.93	1.93	11.8	center points
10	1.93	1.93	11.0	
11	1.93	1.93	12.0	
12	1.93	1.93	12.6	
13	1.93	1.93	12.5	

four corner points, five center points in the cube, and four axial points primarily used to approximate the curvature.[34] The magnitude of α describes the distance between the center and axial points.[34] Mathematically, it is expressed as $\alpha = (2^f)^{1/4}$, where f is denoted as the number of factors in the study.[34,35] In the current study, α = 1.41421, and there is no significant change in the α value in each run. The central points were replicated five times, as shown from runs 9−13 in Table 2. This duplication provides a good estimation and also minimizes experimental errors.[35] However, for a better understanding of the response surface shape, the axial measurements shown from runs 5−8 were conducted four times. To eliminate the effect of systematic error, all the runs in this study were randomized.[36] Furthermore, the filtrate loss volume for each of the 13 runs is also shown in the last column of Table 2. Run 1 contains a minimum concentration of both particles. This run demonstrated the highest fluid loss volume out of all the 13 samples. Run 5 displays the polymeric mud type with no nanoparticles. The fluid loss volume was on the higher side as PAC was unable to successfully plug the pore spaces on the filter paper. Conversely, run 7 demonstrates a nanofluid mud with no polymeric material PAC. The filtrate loss for this mud was <10 mL. The MWCNT/TiO_2 nanoparticles dispersed in the mud sample and performed as a plaster among the different particles present within the mud system. Substantial blocking of the permeation channels present in the mud cake was done by MWCNT/TiO_2 nanoparticles, which eventually reduced the filtrate loss volume from the mud. Moreover, these particles strengthened the mud cake to make it firmer and more homogeneous. The bond between MWCNT/TiO_2 nanoparticles and PAC was well-oriented and was missing when PAC was used as a separate entity. The MWCNT/TiO_2 nanoparticles deposit layer by layer and form a strengthened mud cake, as shown in Figure 4. This phenomenon suppresses the permeability of the mud cake and reduces the fluid loss volume from drilling mud.

Statistical Analysis. Response surface methodology was used to investigate the experimental data set collected from the central composition design. The prediction of fluid loss volume in the API filter press test was done through a second-order polynomial equation, as shown by eq 1.

$$F = n_o + n_1 \times \frac{\text{MWCNT}}{TiO_2} + n_2 \times \text{PAC} + n_3 \times \frac{\text{MWCNT}}{TiO_2} \times \frac{\text{MWCNT}}{TiO_2} + n_4 \times \text{PAC} \times \text{PAC} + n_5 \frac{\text{MWCNT}}{TiO_2} \times \text{PAC}$$

where F denotes the response variable (1)

The current study indicates the fluid loss volume. $\frac{\text{MWCNT}}{TiO_2}$ and PAC are defined as the concentrations of nanoparticles and polymer in the water-based mud system. The variables n_o,n_1,n_2, n_3, n_4, and n_5 represent the linear and quadratic constants. Upon further division, n_o represents the constant coefficient, n_1, and n_2 shows the linear factors;n_3 and n_4 exhibit the quadratic coefficients; and n_5 denotes the interaction effects between $\frac{\text{MWCNT}}{TiO_2}$ and PAC in the model.[37] The response surface plots were generated using MINITAB software. Analysis of variance (ANOVA) was calculated to observe the influence of $\frac{\text{MWCNT}}{TiO_2}$ and PAC on the filtrate loss volume. All of the statistical computations were conducted using MINITAB software.

Analysis of the Quality of the Model. The quality of the model developed by the central composition design was investigated by using graphical error analysis. This analysis is primarily based on the cross-plot. The cross-plot consists of a perfect model line with a unit slope. The equation $y = x$ on the graph represents the perfect model line having a unit slope and y-intercept = 0. The model-predicted values were plotted against the experimental results, and the accuracy of the model was investigated by the accumulation of data set points near the perfect model line.[38] Moreover, the regression coefficient (R^2) was also calculated to examine the quality of the model. A good agreement between the model and experimental result usually yields R^2 closer to 1.[34]

RESULT AND DISCUSSION

Normality Test and Analysis of Residual. To evaluate the performance of the predicted model, we conducted some diagnostic tests conducted. These tests consisted of a normal probability plot, which refers to information about the residual and its frequency. The normality test was conducted with the help of a normal probability plot. This test was conducted to investigate whether the residuals were following the normal probability distribution or not.[36] Points falling onto the straight line indicated that the residual had achieved a normal probability distribution. The residual plots provided information related to the discrepancy between the model and experimental results. According to Figure 5a, the errors associated with the model were normally distributed as they overlapped onto the straight line. A maximum number of red color points depicting the filtration loss volume were located on the straight line, while three points showed a minor deviation from the normal. The linear nature of the graph indicates a closer agreement between the experimental result and the model-predicted result obtained by using the response surface tool. Figure 5b,c shows the residual plots for the given model. Points falling over the 0th line indicate an accurate prediction of the filtrate loss volume from the model. Out of 13 data points, 12 of the predicted results are within ±2 mL. Run

https://doi.org/10.1021/acsomega.4c04177
ACS Omega 2024, 9, 34765−34776

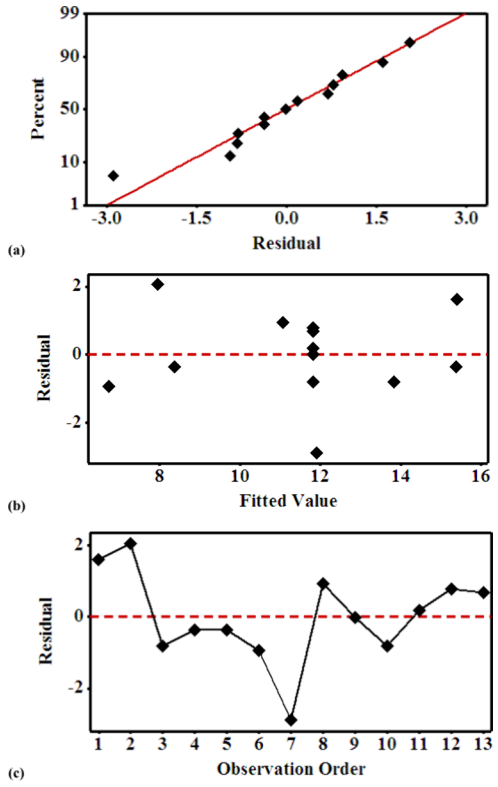

Figure 5. (a–c) Diagnostic plots for filtrate loss volume: (a) normal probability plot, (b) residual plot, and (c) residual versus the number of runs.

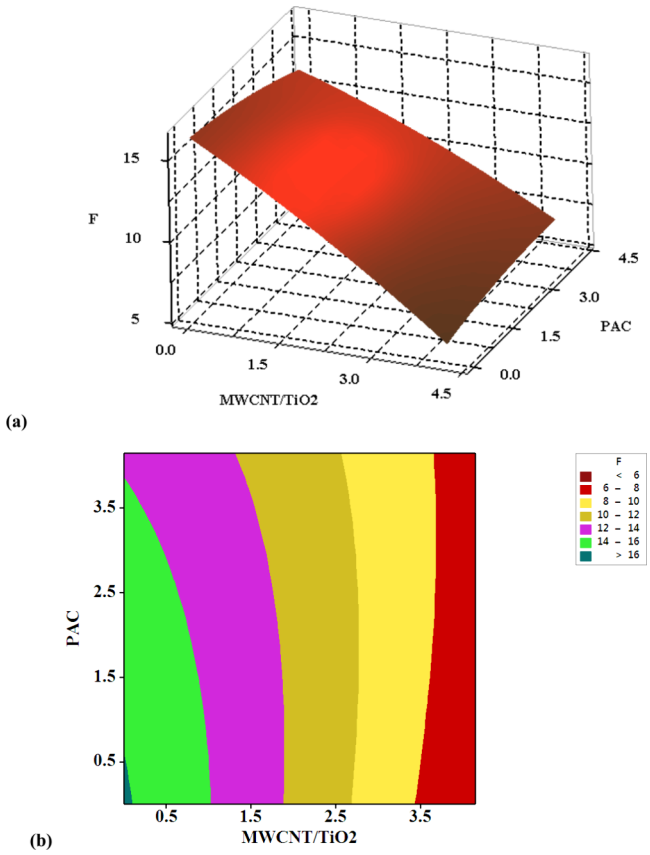

Figure 6. (a,b) Central composition design method: (a) response surface and (b) contour plot analysis for filtrate loss volume.

7, as indicated in Table 2, demonstrated an error greater than the ±2 mL limit. An overprediction of the filtrate loss was observed in this sample. No obvious pattern was recorded in Figure 5c. This analysis clearly shows that the model is adequate with satisfactory performance, and there was no reason to suspect any uncertainty in the model performance. All of the plots were directly obtained from MINITAB software.

Response Surface and Contour Plot Analysis. The relationship between the two particles in the study and their impact on fluid loss volume can be better understood using surface and contour plots respectively. Figure 6a,b shows the surface and contour plot analysis between the filtrate loss and particles of the study. The response surface plots indicate a three-dimensional analysis highlighting the mutual relations between the two variables MWCNT/TiO_2 and PAC and their influence on filtrate loss volume. The two-dimensional elliptical contour in Figure 6b highlights the pairwise interaction between the variables and shows their effect on the fluid filtration loss. According to Figure 6a, it can be noted that the concentration of nanoparticles MWCNT/TiO_2 was more important than the polymer PAC in the mud system. Substantial reduction in the filtrate loss volume was recorded as the concentration of MWCNT/TiO_2 increased in the mud system. Moreover, the concentration of PAC decreases the fluid loss up to some extent, yet the concentration of MWCNT/TiO_2 still plays a prominent role in reducing the fluid loss. The sample with a maximum concentration of MWCNT/TiO_2 = 4.15 g reduces the filtrate loss to 5.8 mL. The highest fluid loss volume was recorded in run 1 with the lowest concentration of MWCNT/TiO_2 = 0.35 g and PAC = 0.35 g. The elliptical contour analysis in Figure 6b validates the results further in 2D space. The higher intensity effect shown by the dark color represents a lower filtrate loss volume. This considerable reduction is mainly due to the addition of MWCNT/TiO_2 nanoparticles; however, the mutual interaction was also significant. This pairwise interactive plot reveals that as the concentration of MWCNT/TiO_2 increases, a substantial reduction in the filtrate loss was noted. Moreover, when the weight percent of MWCNT/TiO_2 was on the lower side, the performance of the PAC was insignificant. Increasing the concentration of PAC while keeping MWCNT/TiO_2 at a lower concentration will not be able to control the fluid loss from the mud system. No distinctive effect was recorded in fluid loss in terms of PAC concentration.

Interactive Plot Analysis. The response surface and contour plots were further validated by the 2D interactive plot, as shown in Figure 7. The MWCNT/TiO_2 demonstrated a negative influence on the filtration characteristics. This impact reveals that as the concentration of MWCNT/TiO_2 decreased in the mud system, an increase in fluid loss was recorded. The particles were responsible for plugging the nanospacing, which eventually reduced the filtrate loss from the mud. Conversely, the polymer PAC showed an insignificant influence on the fluid loss mechanism. In the interactive plot, this polymer is represented by a near horizontal line. This behavior showed that PAC is trivial and has no considerable impact on the fluid loss control. Furthermore, this interactive plot is in good agreement with the contour plot shown in Figure 6b. The long polymeric chain was unable to effectively prevent fluid loss from the mud sample.

https://doi.org/10.1021/acsomega.4c04177
ACS Omega 2024, 9, 34765−34776

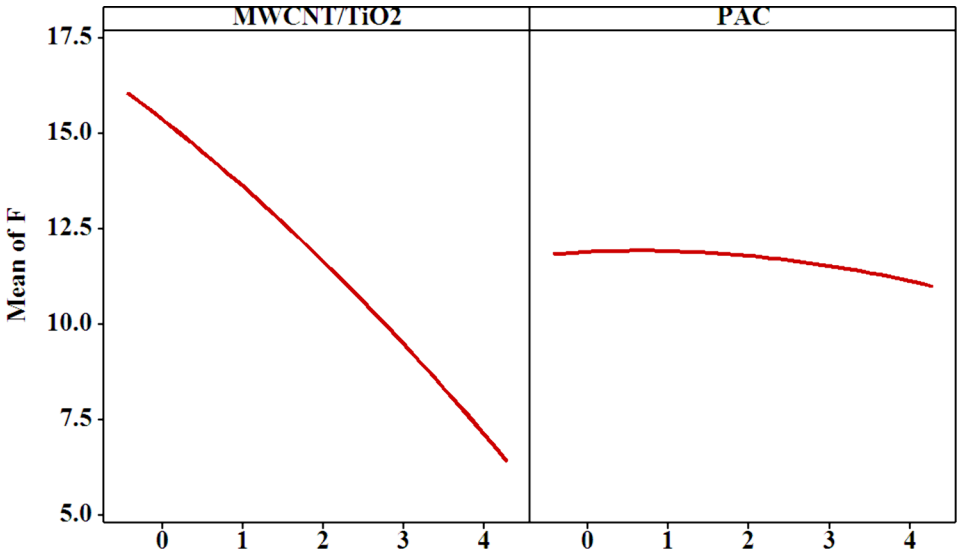

Figure 7. Interactive plot analysis showing the influence of particles on fluid loss volume

Analysis of Variance (ANOVA). Analysis of variance (ANOVA) is the most reliable and basic statistical tool used to evaluate the quality of the fitted model.[39] This statistical parameter was used to investigate the influence of an element or a set of elements on the response variable.[36] Table 3 shows

Table 3. Analysis of Variance (ANOVA) for the Regression Model

source	DF	adjusted SS	adjusted MS	*F*-value	*p*-value
model	5	81.29	16.26	5.77	0.020
linear	2	76.99	38.50	13.65	0.004
$MWCNT/TiO_2$	1	76.36	76.36	27.08	0.001
PAC	1	0.590	0.590	0.21	0.661
square	2	0.526	0.263	0.09	0.912
$MWCNT/TiO_2$*$MWCNT/TiO_2$	1	0.373	0.373	0.13	0.727
PAC*PAC	1	0.177	0.177	0.06	0.809
two-way interaction	1	1	1	0.35	0.570
$MWCNT/TiO_2$*PAC	1	1	1	0.35	0.570

the ANOVA result consisting of *F* and *p*-values for the regression model. The model Fisher's *F*-test value of 5.77 and *p*-value of 0.020 (<0.05) indicate that the regression model is highly significant. The regression model is efficient in providing the relationship between the two studied particles ($MWCNT/TiO_2$and PAC) and the filtrate loss volume. Moreover, the coefficient of R^2 = 0.8446 was also provided by the model. This parameter shows that only 84.46% of the total variations in the experimental results were explicated by the model. However, 17.54% of the data were not explained by the regression model. From Table 3, it is evident that the $MWCNT/TiO_2$ parameter was the most significant parameter with *p*-value < 0.05. This explains why $MWCNT/TiO_2$ particles play a substantial role in minimizing fluid loss. However, the PAC *p*-value > 0.05, thus indicating its trivial effect on fluid loss. Moreover, the two-way interaction and the square features were all considered insignificant in this regression model.

Validation of the RSM Model. The regression equation formed by the model in the uncoded units is shown in eq 2. The variables n_o, n_1, n_2, n_3, n_4, and n_5 represent the linear and quadratic constants present in eq 2. On the basis of the equation, a cross-plot was developed, as shown in Figure 8, which was used to further investigate the accuracy of the model by graphical means.

$$F = 16.20 - 2.04 \times \frac{MWCNT}{TiO_2} - 0.30 \times PAC - 0.10 \times 2 \times \frac{MWCNT}{TiO_2} \times \frac{MWCNT}{TiO_2} - 0.071 \times PAC \times PAC + 0.202 \frac{MWCNT}{TiO_2} \times PAC \quad (2)$$

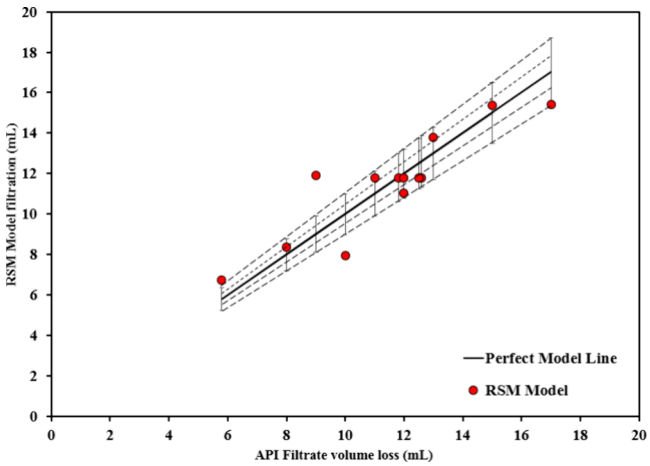

Figure 8. Cross-plot between the model and experimental.

The straight line represents the perfect model line $y = x$. Points falling on this line specify the accurate prediction of the regression model. The two inner lines represent the ±5% error percentage, while the outer lines display ±10%. It is evident from Figure 8 that 10 out of 13 data set points fall under the ±10% error window, thus indicating 77.61% accuracy of the regression model. The two outer points are associated with runs 2, 6, and 7 and display 16%, 20%, and 32% of the errors, respectively. Figure 9 shows the radar plot displaying the

https://doi.org/10.1021/acsomega.4c04177
ACS Omega 2024, 9, 34765−34776

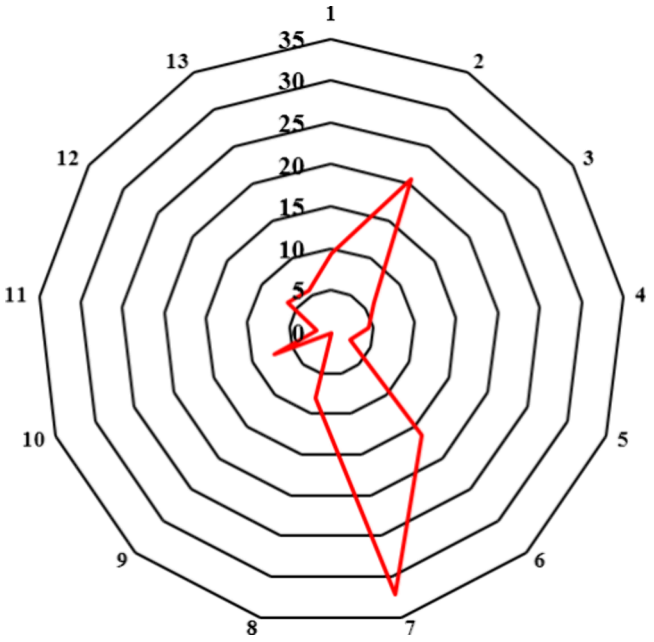

Figure 9. Radar plot of residual error.

residual error associated with each run of the experiment. The maximum errors are 32% followed by 20% and 16% in runs 7, 6, and 2, respectively. All the remaining filtrate volume obtained from eq 2 is below 10%.

Mechanism of Filtration Control. Figure 10 shows the mechanism of filtrate loss control with nanoparticles and polymers. Figure 10a shows the loss of mud in the formation. In the current state, there are no polymers or nanoparticles within the mud system. Therefore, a high volume of filtrate loss with a greater thickness of mud cake can be observed. When the two entities of polymers and nanoparticles become part of the mud system, a smooth, thin, and compacted mud cake is formed on the face of the formation. Moreover, these nanoparticles plug the pore spaces and prevent the flow of water into the formation.[40] Moreover, the addition of MWCNT/TiO_2 particles increases the viscosity, which causes a decrease in the filtration rate. Conversely, the addition of polymers affects the microstructure of the mud cake.[33] Polymers tend to form cross-linked polymeric chains that improve the filtration behavior of the mud. Furthermore, the polymers adsorb on the surface of the formation, and the functional group linked with them prevents the migration of water into the formation, as shown in Figure 10b.

CONCLUSION

In this current study, the influence of polymer and nanoparticles in controlling the fluid loss from the water-based mud system was investigated using the central composite response surface design of experiment. Thirteen samples of WBMs consisting of different concentrations of PAC and MWCNTs/TiO_2 nanoparticles were formulated and examined for the fluid loss volume. The concentration of the two particles was the major factor used in the design of the experiment. The following findings were drawn from the investigation:

1. Concentration of MWCNTs/TiO_2 played a significant role in minimizing the fluid loss volume.
2. According to ANOVA analysis, the interaction between the two entities, PAC and MWCNTs/TiO_2, was not significant. MWCNTs/TiO_2, as a separate entity, was effective in controlling the fluid loss from the mud.
3. On the basis of the interactive plots, the MWCNT/TiO_2 demonstrated a negative influence on the filtration characteristics. A decrease in concentration will cause an increase in the fluid loss volume. This particle was responsible for plugging the nanospacing, which eventually reduced the filtrate loss.
4. The maximum errors recorded were 32% followed by 20% and 16% in runs 7, 6, and 2, respectively. Ten out of 13 data set points fell under the ±10% error window, thus indicating 77.61% accuracy of the regression model.

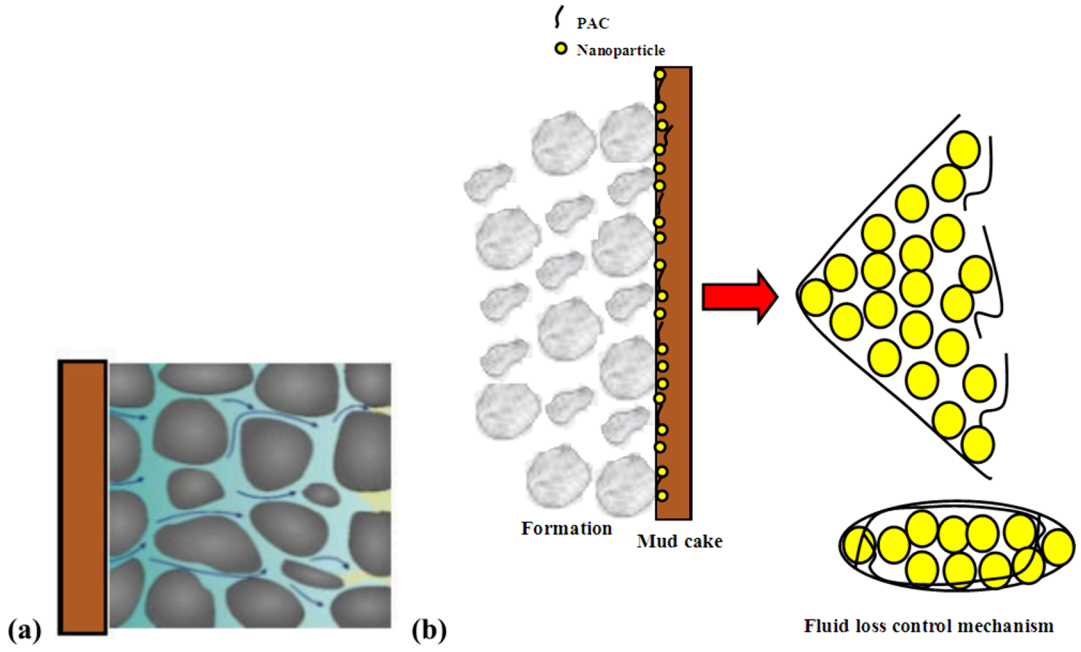

Figure 10. Mechanism of filtrate loss control (a) without nanoparticles and polymers and (b) with nanoparticles and polymers.

https://doi.org/10.1021/acsomega.4c04177
ACS Omega 2024, 9, 34765−34776

5. The pairwise interactive plot reveals that increasing the concentration of PAC while keeping MWCNT/TiO_2 at a lower concentration will not minimize the fluid loss from the mud system.

On the basis of all of the statistical measurements, the predicted results from CCD were in good agreement with the API filtrate loss test. It can further confirm that the MWCNT/TiO_2 was far superior in minimizing the fluid loss from the WBM system than PAC.

RECOMMENDATIONS FOR FUTURE WORK DIRECTIONS

The research conducted in this article highlights the application of composite nanoparticles in the petroleum sector. The particles were extremely efficient in minimizing the fluid loss volume from the base mud. Following are the recommendations for future work directions with these particles:

1. The MWCNT/TiO_2 composite can further be tested at high-temperature and pressure conditions. These conditions replicate the actual environments that are usually present beneath the subsurface.
2. In the current work, anatase-TiO_2 was composited with MWCNTs. However, other forms of titanium dioxide nanoparticles, such as brookite and rutile, can also be examined, and their influence on fluid loss testing can be explored.
3. The environmental effect of these particles is another important area that needs further investigation.
4. The interaction of these particles with other drilling fluid additives needs auxiliary research. This analysis will eventually assist in evaluating the stability and efficiency of this composite in different environments.

AUTHOR INFORMATION

Corresponding Author

Mei-Chun Li − *China University of Petroleum (East China), Qingdao City 266580 Shandong Province, China; State Key Laboratory of Deep Oil and Gas, China University of Petroleum (East China), Qingdao 266580, China;* orcid.org/0000-0001-9381-0093; Email: mli@upc.edu.cn

Authors

Muhammad Arqam Khan − *China University of Petroleum (East China), Qingdao City 266580 Shandong Province, China; Department of Petroleum Engineering, NED University of Engineering and Technology, Karachi 75270, Pakistan;* orcid.org/0000-0001-8665-7705

Shaine Mohammadali Lalji − *Department of Petroleum Engineering, NED University of Engineering and Technology, Karachi 75270, Pakistan*

Syed Imran Ali − *Department of Petroleum Engineering, NED University of Engineering and Technology, Karachi 75270, Pakistan;* orcid.org/0000-0003-0133-9455

Muneeb Burney − *MOL Pakistan Oil and Gas Company Ltd. B.V, Islamabad 75400, Pakistan*

Complete contact information is available at: https://pubs.acs.org/10.1021/acsomega.4c04177

Notes

The authors declare no competing financial interest.

ACKNOWLEDGMENTS

This work was supported by the Natural Science Foundation of Shandong Province (ZR2023ME131), the Basic Science Center Project of the National Natural Science Foundation of China (52288101) "Flow Control of Ultra-deep and Extra-deep Oil and Gas Drilling", and the Jiangsu Specially-Appointed Professor Program.

ABBREVIATION

PAC	polyanionic cellulose
WBM	water-based mud
OBM	oil-based mud
CCD	central composite design
MWCNT	multiwalled carbon nanotubes
TiO_2	titanium dioxide
ANOVA	analysis of variance

REFERENCES

(1) Li, X.; Jiang, G.; Shen, X.; Li, G. Poly-l-arginine as a High-Performance and Biodegradable Shale Inhibitor in Water-Based Drilling Fluids for Stabilizing Wellbore. *ACS Sustainable Chem. Eng.* **2020**, *8* (4), 1899−1907.

(2) Rezaei, A.; Nooripoor, V.; Shahbazi, K. Applicability of Fe3O4 nanoparticles for improving rheological and filtration properties of bentonite-water drilling fluids in the presence of sodium, calcium, and magnesium chlorides. *J. Petrol Explor Prod Technol.* **2020**, *10*, 2453−2464.

(3) Lalji, S. M.; Ali, S. I.; Haneef, J.; et al. Changes in Pakistan crude oil properties contaminated by water-based drilling fluids with varying KCL concentrations. *Chem. Pap* **2022**, *76*, 4189−4201.

(4) Elkatatny, S. Enhancing the Rheological Properties of Water-Based Drilling Fluid Using Micronized Starch. *Arab J. Sci. Eng.* **2019**, *44*, 5433−5442.

(5) Bayat, A. E.; Jalalat Moghanloo, P.; Piroozian, A.; Rafati, R. Experimental investigation of rheological and filtration properties of water-based drilling fluids in presence of various nanoparticles. *Colloids Surf., A* **2018**, *555*, 256−263.

(6) Aftab, A.; Ismail, A.R.; Ibupoto, Z.H.; Akeiber, H.; Malghani, M.G.K. Nanoparticles based drilling muds a solution to drill elevated temperature wells: A review. *Renewable Sustainable Energy Rev.* **2017**, *76*, 1301−1313.

(7) Lalji, S. M.; Ali, S. I.; Awan, Z. U. H.; et al. A novel technique for the modeling of shale swelling behavior in water-based drilling fluids. *J. Petrol Explor Prod Technol.* **2021**, *11*, 3421−3435.

(8) Rasool, M. H.; Zamir, A.; Elraies, K. A.; et al. Rheological characterization of potassium carbonate deep eutectic solvent (DES) based drilling mud. *J. Petrol Explor Prod Technol.* **2022**, *12*, 1785−1795.

(9) Sami, N. A. Effect of magnesium salt contamination on the behavior of drilling fluids. *Egyptian Journal of Petroleum* **2016**, *25*, 453.

(10) Chang, W.-Z.; Leong, Y.-K. Ageing and collapse of bentonite gels—effects of Li, Na, K and Cs ions. *Rheol. Acta* **2014**, *53*, 109−122.

(11) Lam, C.; Martin, P. J.; Jefferis, S. A. Rheological Properties of PHPA Polymer Support Fluids. *J. Mater. Civ. Eng.* **2015**, *27* (11), 04015021.

(12) Lalji, S. M.; Ali, S. I.; Asad, M. Experimental Effect of Biopolymers, Synthetic and Modified Polymers on Western Pakistan Shale (GHAZIJ) Stability. *Arab J. Sci. Eng.* **2023**, *48*, 16639.

(13) Siqueira, G.; Bras, J.; Dufresne, A. Cellulosic Bionanocomposites: A Review of Preparation, Properties and Applications. *Polymers* **2010**, *2* (4), 728−765.

(14) Jia, X.; Zhao, X.; Chen, B.; Egwu, S. B.; Huang, Z. Polyanionic cellulose/hydrophilic monomer copolymer grafted silica nanocomposites as HTHP drilling fluid-loss control agent for water-based drilling fluids. *Appl. Surf. Sci.* **2022**, *578*, 152089.

(15) Iscan, A. G.; Kok, M. V. Effects of Polymers and CMC Concentration on Rheological and Fluid Loss Parameters of Water-

Based Drilling Fluids. *Energy Sources, Part A: Recovery, Utilization, and Environmental Effects* **2007**, *29* (10), 939−949.
(16) Mahto, V.; Sharma, V.P. Rheological study of a water based oil well drilling fluid. *J. Pet. Sci. Eng.* **2004**, *45* (1−2), 123.
(17) Aftab, A.; Ismail, A.R.; Khokhar, S.; Ibupoto, Z.H. Novel zinc oxide nanoparticles deposited acrylamide composite used for enhancing the performance of water-based drilling fluids at elevated temperature conditions. *J. Pet. Sci. Eng.* **2016**, *146*, 1142−1157.
(18) Al-saba, M. T.; Al Fadhli, A.; Marafi, A.; Hussain, A.; Bander, F.; Al Dushaishi, M. F. Application of Nanoparticles in Improving Rheological Properties of Water Based Drilling Fluids. In *SPE Kingdom of Saudi Arabia Annual Technical Symposium and Exhibition*, Dammam, Saudi Arabia, April 23−26, 2018; SPE-192239-MS. DOI: 10.2118/192239-MS.
(19) Abdo, J.; Zaier, R.; Hassan, E.; AL-Sharji, H.; Al-Shabibi, A. ZnO−clay nanocomposites for enhance drilling at HTHP conditions. *Surf. Interface Anal.* **2014**, *46*, 970−974.
(20) Ghayedi, A.; Khosravi, A. Laboratory investigation of the effect of GO-ZnO nano-composite on drilling fluid properties and its potential on H2S removal in oil reservoirs. *J. Pet. Sci. Eng.* **2020**, *184*, 106684.
(21) Alvi, M. A. A.; Belayneh, M.; Bandyopadhyay, S.; Minde, M. W. Effect of Iron Oxide Nanoparticles on the Properties of Water-Based Drilling Fluids. *Energies* **2020**, *13*, 6718.
(22) Ponmani, S.; Nagarajan, R.; Sangwai, J. S. Effect of Nanofluids of CuO and ZnO in Polyethylene Glycol and Polyvinylpyrrolidone on the Thermal, Electrical, and Filtration-Loss Properties of Water-Based Drilling Fluids. *SPE J.* **2016**, *21*, 405−415.
(23) Sadeghalvaad, M.; Sabbaghi, S. The effect of the TiO2/polyacrylamide nanocomposite on water-based drilling fluid properties. *Powder Technol.* **2015**, *272*, 113−119.
(24) Mohideen, A. A. M.; Saheed, M. S. M.; Mohamed, N. M. Multiwalled carbon nanotubes and graphene oxide as nano-additives in water-based drilling fluid for enhanced fluid-loss-control & gel strength. *AIP Conf. Proc.* **2019**, *2151*, 020001.
(25) Beg, M.; Kumar, P.; Choudhary, P.; Sharma, S. Effect of high temperature ageing on TiO2 nanoparticles enhanced drilling fluids: A rheological and filtration study. *Upstream Oil and Gas Technology* **2020**, *5*, 100019.
(26) Reghunath, S.; Pinheiro, D.; KR, S. D. A review of hierarchical nanostructures of TiO2: Advances and applications. *Applied Surface Science Advances* **2021**, *3*, 100063.
(27) Omri, A.; Benzina, M. Influence of the origin of carbon support on the structure and properties of TiO2 nanoparticles prepared by dip coating method. *Arabian Journal of Chemistry* **2019**, *12* (8), 2926−2936.
(28) Okoro, E. E.; Zuokumor, A. A.; Okafor, I. S.; et al. Determining the optimum concentration of multiwalled carbon nanotubes as filtrate loss additive in field-applicable mud systems. *J. Petrol Explor Prod Technol.* **2020**, *10*, 429−438.
(29) Mehra, N. K.; Mishra, V.; Jain, N.K. A review of ligand tethered surface engineered carbo nanotubes. *Biomaterials* **2014**, *35* (4), 1267−1283.
(30) Veza, I.; Spraggon, M.; Fattah, I.M. R.; Idris, M. Response surface methodology (RSM) for optimizing engine performance and emissions fueled with biofuel: Review of RSM for sustainability energy transition. *Results Eng.* **2023**, *18*, 101213.
(31) Muduli, S.; Lee, W.; Dhas, V.; Mujawar, S.; Dubey, M.; Vijayamohanan, K.; Han, S.-H.; Ogale, S. Enhanced Conversion Efficiency in Dye-Sensitized Solar Cells Based on Hydrothermally Synthesized TiO2−MWCNT Nanocomposites. *ACS Appl. Mater. Interfaces* **2009**, *1* (9), 2030−2035.
(32) Lalji, S. M.; Haneef, J.; Hashmi, S. Mitigating Paleocene age Ranikot shale formation swelling characteristics using carbon supported anatase-titanium dioxide (MWCNT/TiO2, GO/TiO2 and AC/TiO2) nanomaterial water-based mud—chemical and rock interaction study. *Chem. Pap* **2024**, *78*, 4361−4381.
(33) Rafieefar, A.; Sharif, F.; Hashemi, A.; Bazargan, A. M. Rheological Behavior and Filtration of Water-Based Drilling Fluids Containing Graphene Oxide: Experimental Measurement, Mechanistic Understanding, and Modeling. *ACS Omega* **2021**, *6* (44), 29905−29920.
(34) Lee, T. Z. E.; Krongchai, C.; Mohd Irwn Lu, N. A. L.; et al. Application of central composite design for optimization of the removal of humic substances using coconut copra. *Int. J. Ind. Chem.* **2015**, *6*, 185−191.
(35) Ferella, F.; Mazziotti Di Celso, G.; De Michelis, I.; Stanisci, V.; Veglio, F. Optimization of the transesterification reaction in biodiesel production. *Fuel* **2010**, *89* (1), 36−42.
(36) Ghelich, R.; Jahannama, M. R.; Abdizadeh, H.; Torknik, F. S.; Vaezi, M. R. Central composite design (CCD)-Response surface methodology (RSM) of effective electrospinning parameters on PVP-B-Hf hybrid nanofibrous composites for synthesis of HfB2-based composite nanofibers. *Composites, Part B* **2019**, *166*, 527−541.
(37) Alhajabdalla, M.; Mahmoud, H.; Nasser, M. S.; Hussein, I. A.; Ahmed, R.; Karami, H. Application of Response Surface Methodology and Box−Behnken Design for the Optimization of the Stability of Fibrous Dispersion Used in Drilling and Completion Operations. *ACS Omega* **2021**, *6* (4), 2513−2525.
(38) Ali, S. I.; Lalji, S. M.; Haneef, J.; Ahsan, U.; Khan, M. A.; Yousaf, N. Estimation of asphaltene adsorption on MgO nanoparticles using ensemble learning. *Chemom. Intell. Lab. Syst.* **2021**, *208*, 104220.
(39) Iqbal, M.; Iqbal, N.; Bhatti, I. A.; Ahmad, N.; Zahid, M. Response surface methodology application in optimization of cadmium adsorption by shoe waste: A good option of waste mitigation by waste. *Ecological Engineering* **2016**, *88*, 265−275.
(40) Zhang, H.; Zhong, Y.; She, J.; et al. Experimental study of nano-drilling fluid based on nano temporary plugging technology and its application mechanism in shale drilling. *Appl. Nanosci* **2019**, *9*, 1637−1648.

https://doi.org/10.1021/acsomega.4c04177
ACS Omega 2024, 9, 34765−34776